Bioorg. Med. Chem. Lett. 43 (2021) 128048

Contents lists available at ScienceDirect

Bioorganic & Medicinal Chemistry Letters

journal homepage: www.elsevier.com/locate/bmcl

Discovery of 1-[2-(1-methyl-1H-pyrazol-5-yl)-[1,2,4]triazolo[1,5-*a*]pyridin-6-yl]-3-(pyridin-4-ylmethyl)urea as a potent NAMPT (nicotinamide phosphoribosyltransferase) activator with attenuated CYP inhibition

Mayuko Akiu [a,*], Takashi Tsuji [a], Yoshitaka Sogawa [a], Koji Terayama [a], Mika Yokoyama [a], Jun Tanaka [a], Daigo Asano [a], Ken Sakurai [a], Eduard Sergienko [b], E. Hampton Sessions [b], Stephen J. Gardell [c], Anthony B. Pinkerton [b], Tsuyoshi Nakamura [a]

[a] *R&D Division, Daiichi Sankyo Co., Ltd., 1-2-58 Hiromachi, Shinagawa-ku, Tokyo 140-8710, Japan*
[b] *Sanford Burnham Prebys Medical Discovery Institute, 10901 North Torrey Pines Road, La Jolla, CA 92037, USA*
[c] *Translational Research Institute, AdventHealth, Orlando, FL 32804, USA*

ARTICLE INFO

Keywords:
NAMPT activators
NAD^+
Triazolopyridines
CYP inhibition
Log*D*

ABSTRACT

Nicotinamide phosphoribosyltransferase (NAMPT) catalyzes the rate-limiting step of the NAD^+ salvage pathway. Since NAD^+ plays a pivotal role in many biological processes including metabolism and aging, activation of NAMPT is an attractive therapeutic target for treatment of diverse array of diseases. Herein, we report the continued optimization of novel urea-containing derivatives which were identified as potent NAMPT activators. Early optimization of HTS hits afforded compound **12**, with a triazolopyridine core, as a lead compound. CYP direct inhibition (DI) was identified as an issue of concern, and was resolved through modulation of lipophilicity to culminate in 1-[2-(1-methyl-1H-pyrazol-5-yl)-[1,2,4]triazolo[1,5-*a*]pyridin-6-yl]-3-(pyridin-4-ylmethyl)urea (**21**), which showed potent NAMPT activity accompanied with attenuated CYP DI towards multiple CYP isoforms.

Introduction

Nicotinamide adenine dinucleotide (NAD^+) is a key cellular factor which plays an important role in intermediary metabolism.[1,2] NAD^+ possesses a nicotinamide moiety as the site of a redox reaction, which makes it an important coenzyme for hydride transfer enzymes essential for metabolic processes including glycolysis, the TCA cycle and oxidative phosphorylation.[3–7] NAD^+ is also an important cosubstrate for certain enzymes, such as sirtuins (SIRTs), poly (ADP-ribose) polymerases (PARPs), and cyclic ADP-ribose (cADPR) synthases (CD38 and CD157).[3–7] Based on these multi-faceted functions, several studies suggest that increasing tissue levels of NAD^+ mediate beneficial effects toward wide range of diseases, such as metabolic disorders,[8] cardiovascular and kidney disease,[9–11] mitochondria disease,[12] neurodegeneration,[13–15] stroke, [16,17] retinal degeneration,[18,19] or muscle wasting disorder.[20–22]

Ongoing NAD^+ biosynthesis is necessary to preserve the NAD^+ level, given that NAD^+ as a cosubstrate contributes as a donor of ADP-ribose, which involves the hydrolysis of linkage between nicotinamide (NAM) and the ADP-ribosyl moieties. NAD^+ is synthesized by two major pathways; the *de novo* pathway originating from tryptophan, and *via* salvage pathway from NAM, which is the dominant pathway in most mammals.[3–7] In the salvage pathway, NAM is converted to NAM mononucleotide (NMN) by the enzyme nicotinamide phosphoribosyltransferase (NAMPT), the putative rate-limiting step of this salvage pathway,[1–5] which is a homo-dimeric type II phosphoribosyl transferase.[23] NMN is subsequently converted into NAD^+ by various nicotinamide mononucleotide adenylyltransferases (NMNATs).[3–7] In one study, overexpression of NAMPT in skeletal muscle resulted in an increase in NAD^+ levels, leading to improved exercise endurance and metabolic abnormalities in mice.[22] Accordingly, activation of NAMPT enzyme would elicit elevation of NAD^+ level ultimately leading to modulation or enhancement of metabolism, and thus would offer therapeutic avenues for multiple diseases associated with NAD^+ deficiency. Herein, we report the further optimization of series of compounds possessing a (pyridin-4-ylmethyl) urea moiety.

* Corresponding author.
E-mail address: akiu.mayuko.bs@daiichisankyo.co.jp (M. Akiu).

https://doi.org/10.1016/j.bmcl.2021.128048
Received 8 February 2021; Received in revised form 9 April 2021; Accepted 14 April 2021
Available online 19 April 2021

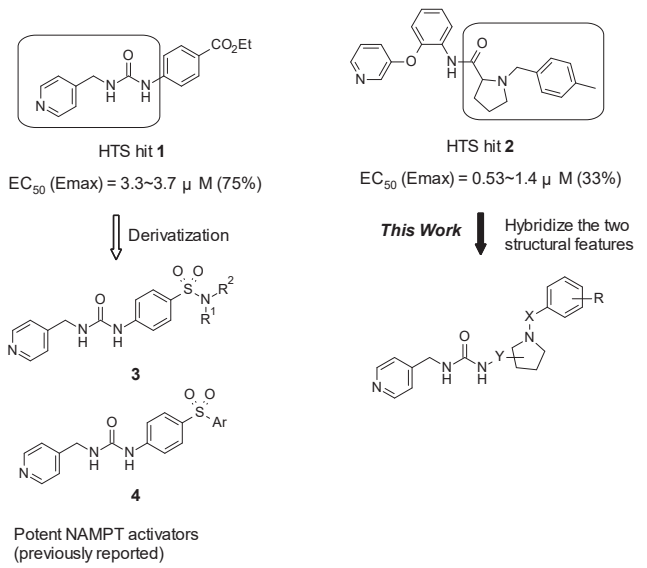

Fig. 1. Design principles of novel NAMPT activators.

Table 1
Initial SAR exploration.

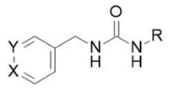

Cpd	R	X	Y	NAMPT Enzyme assay (EC_{50} / Emax)	Cell-based assay[a] (HEK293A) (%@1, 3, 10 μM)
5	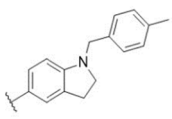	N	CH	63%@100 μM[b]	NT[c]
6	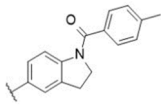	N	CH	0.48 μM/ 91%	25, 45, 62
7	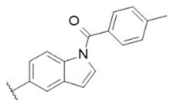	N	CH	0.22 μM/ 55%	44, 76, 89
8	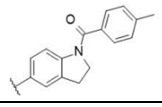	CH	N	IC_{50} 0.032 μM	NT[c]

[a] Percentage indicates the amount of NAD^+ increase achieved with 1, 3, 10 μM of the compound, compared to that achieved with 30 μM of compound **1.**
[b] Percentage indicates the amount of NAMPT activation achieved with 100 μM of the compound, compared to that achieved with 30 μM of compound **1.**
[c] Not tested.

Our HTS campaign, which utilized a fluorescence thermal shift assay followed by an enzymatic assay using purified NAMPT, led to the identification of urea compound **1** as well as proline compound **2** as hit compounds that led to a moderate enhancement of NAMPT activity.[24] The NAMPT activation activity of the compounds were determined by measuring the EC_{50} and Emax (maximal NAMPT activation) as described previously.[24,25] While the urea compound **1** exhibited a fairly high Emax of 75%, the proline compound **2** was more potent, with an

Table 2
Exploration of 6–5 bicyclic cores.

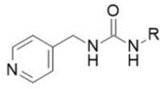

Cpd	R	NAMPT Enzyme assay (EC_{50} / Emax)	Cell-based assay[a] (HEK293A) (%@1, 3, 10 μM)
9	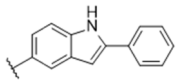	0.51 μM/ 103%	73, 107, 131
10	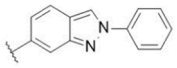	0.040 μM/ 155%	121, 150, 176
11	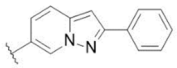	0.012 μM/ 135%	115, 148, 145
12	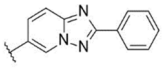	0.083 μM/ 131%	130, 139, 161

[a] Percentage indicates the amount of NAD^+ increase achieved with 1, 3, 10 μM of the compound, compared to that achieved with 30 μM of compound **1.**

Table 3
Physicochemical and *in vitro* ADME properties of selected 6–5 bicyclic analogs.

Cpd	log*D*[a]	PAMPA permeability (pH 5.0, pH 7.4) (nm/ s)	Solubility (pH 1.2, 6.8) (μg/mL)	Metabolic Stability[b] (h, mou) (%)	CYP DI[c] (1A2/ 2C9/ 2D6/ 3A4) (%)
10	3.2	46.0, >50	Insoluble[d]	87, 83	88/ 74/ 50/ 75
11	3.5	>50, >50	640, 0.5	83, 91	81/ 78/ 70/ 53
12	3.0	14.2, 27.6	>680, 92	95, 86	63/ 79/ 21/ 37

[a] The distribution coefficients (log*D*) were measured between 1-octanol and phosphate buffered saline (pH 7.4).
[b] The % remaining value at 1 μM concentration of compounds reacted with human or mouse microsomes for 30 min.
[c] The % inhibition value at 10 μM concentration of compounds reacted with corresponding CYP isoforms for 10 min.
[d] Solubility could not be determined because the compound was insoluble to DMSO.

Table 4
Exploration of left-hand region of triazolopyridines.

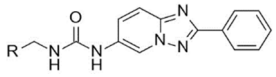

Cpd	R	NAMPT Enzyme assay (EC_{50}/ Emax)	Cell-based assay[a] (HEK293A) (%@1, 3, 10 μM)	CYP DI[b] (1A2/ 2C9/2D6/ 3A4) (%)
13		0.022 μM/ 217%	118, 154, 174	86/ 59/ 23/ 0
14		0.14 μM/ 87%	103, 123, 138	69/ 59/ 13/ 0

[a] Percentage indicates the amount of NAD^+ increase achieved with 1, 3, 10 μM of the compound, compared to that achieved with 30 μM of compound **1.**
[b] The % inhibition value at 10 μM concentration of compounds reacted with corresponding CYP isoforms for 10 min.

Table 5
Exploration of right-hand region of triazolopyridines.

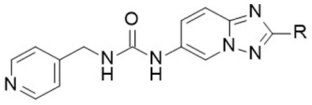

Cpd	R	NAMPT Enzyme assay (EC_{50} / Emax)	Cell-based assay [a] (HEK293A) (%@1, 3, 10 μM)	CYP DI[b] (1A2/ 2C9/ 2D6/ 3A4) (%)	log*D*[c]
15		0.070 μM/ 120%	108, 115, 99	43/ 78/ 50/ 65	3.4
16	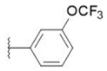	0.35 μM/ 124%	61, 103, 127	28/ 90/ 36/ 0	4.3
17	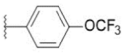	>100 μM	NT[d]	8/ 81/ 24/ 0	4.4
18		5.8 μM/ 101%	0, 32, 55	NT[d]	NT[d]
19	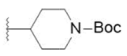	2.4 μM/ 75%	16, 29, 69	NT[d]	NT[d]
20		0.12 μM/ 153%	88, 115, 150	51/ 75/ 27/ 40	2.6
21		0.18 μM/ 132%	71, 107, 150	15/ 42/ 16/ 25	1.8
22		0.19 μM/ 117%	102, 135, 133	12/ 79/ 17/ 4	2.8
23		0.083 μM/ 105%	73, 108, 88	6/ 44/ 13/ 18	1.5

[a] Percentage indicates the amount of NAD^+ increase achieved with 1, 3, 10 μM of the compound, compared to that achieved with 30 μM of compound **1.**
[b] The % inhibition value at 10 μM concentration of compounds reacted with corresponding CYP isoforms for 10 min.
[c] The distribution coefficients (log*D*) were measured between 1-octanol and phosphate buffered saline (pH 7.4).
[d] Not tested.

EC_{50} range (0.53–1.4 μM) but a lower Emax. We previously reported intensive derivatization around **1**, which led to the discovery of potent NAMPT activators such as sulfonamides **3** and sulfones **4**.[24–28] Concurrently, we conducted an initial structure activity relationship (SAR) study around the HTS hit **2**, but the SAR was narrow, with only minor structural variations resulting in a loss of activity (data not shown). We therefore attempted to hybridize the two structural features of **1** and **2**, in anticipation of acquiring a potent novel scaffold. Herein, we report the results of those efforts, which culminated in the discovery of 1-(2-phenyl-[1,2,4]triazolo[1,5-*a*]pyridin-6-yl)-3-(pyridin-4-ylmethyl)urea (**12**) and 1-[2-(1-methyl-1H-pyrazol-5-yl)-[1,2,4]triazolo[1,5-*a*]pyridin-6-yl]-3-(pyridin-4-ylmethyl)urea (**21**) with a triazolopyridine core structure, which displayed potent activities in NAMPT enzyme and cell-based assays (Fig. 1).

The test compounds in Tables 1–5 were synthesized following the general procedures described in Schemes 1-6.

The general procedure for the synthesis of triazolopyridine derivatives is depicted in Scheme 1. The triazolopyridine core structure of

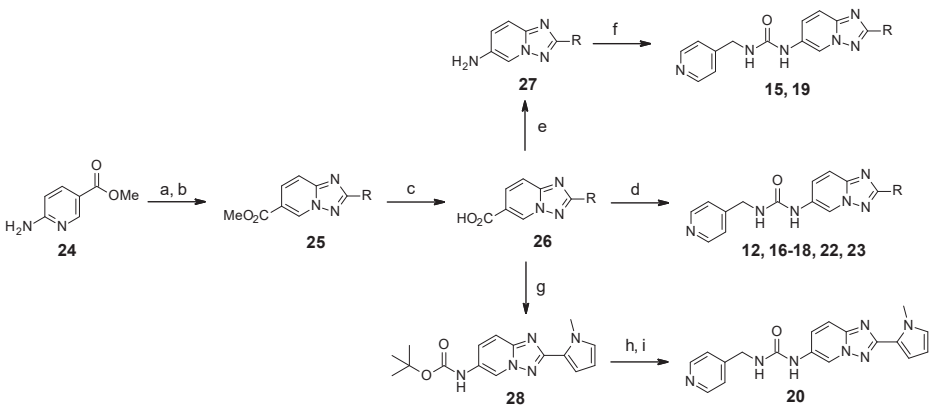

Scheme 1. Synthesis of tiazolopyridine derivatives. Reagents and conditions: (a) Ethyl O-mesitylsulfonylacetohydroxamate, pyridine, perchloric acid, dichloromethane, 91%; (b) RCOCl, pyridine, 80 °C, 36–71%; or RCO_2H, EDCI, HOAt, triethylamine, dichloromethane, 50–89%; (c) 2 M NaOHaq, methanol, THF, 65%-quant.; (d) DPPA, triethylamine, dioxane, 80 °C, then 4-picolylamine, 14–39%; (e) DPPA, triethylamine, DMF, then H_2O, 80 °C, 23–29%; (f) 4-Nitrophenyl [(pyridin-4-yl)methyl] carbamate,[30] DIPEA, 1,4-dioxane, 80 °C, 38–61%; (g) DPPA, triethylamine, CH_2Cl_2, then *t*-butylalcohol, toluene, 100 °C, 74%; (h) 4 M HCl in dioxane, CH_2Cl_2; (i) 4-Nitrophenyl [(pyridin-4-yl)methyl] carbamate, DIPEA, 1,4-dioxane, 80 °C, 67% over two steps.

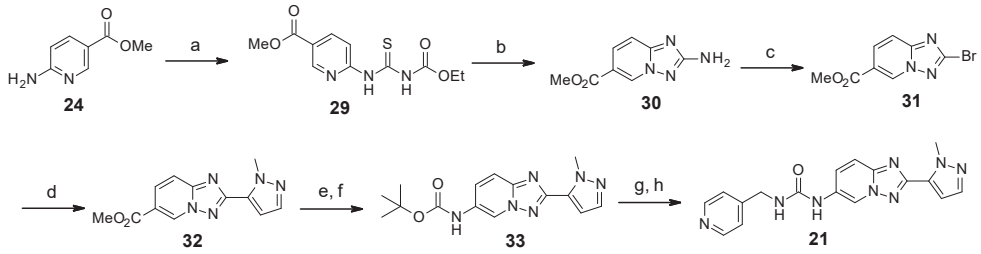

Scheme 2. Synthesis of compound **21**. Reagents and conditions: (a) Ethoxycarbonyl isothiocyanate, dioxane, 50 °C, 66%; (b) Hydroxylammonium chloride, DIPEA, methanol, ethanol, 87%; (c) *t*-Butyl nitrite, copper (II) bromide, acetonitrile, 50 °C, 58%; (d) 1-Methyl-1H-pyrazole-5-boronic acid pinacol ester, [1,1′-bis(diphenylphosphino)ferrocene]palladium(II) dichloride dichloromethane adduct, potassium carbonate, dioxane, H_2O, 60 °C, 45%; (e) 2 N NaOHaq, methanol, THF, 60%; (f) DPPA, triethylamine, CH_2Cl_2, then *t*-butylalcohol, toluene, 100 °C, 76%; (g) 4 M HCl in dioxane, CH_2Cl_2; (h) Triphosgene, triethylamine, 4-picolylamine, dichloromethane, 29% over two steps.

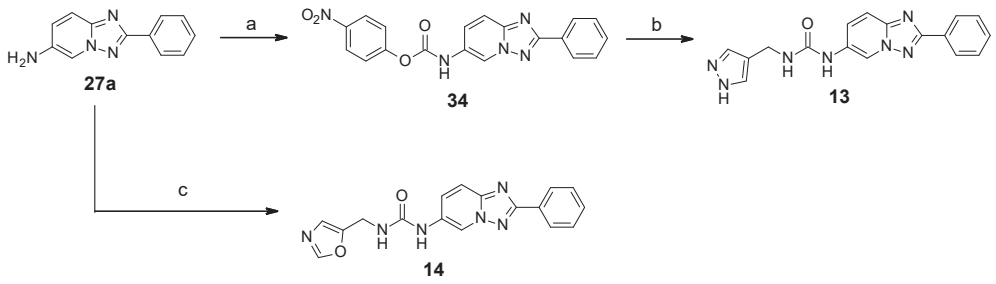

Scheme 3. Synthesis of compounds **13** and **14**. Reagents and conditions: (a) 4-Nitrophenyl chloroformate, toluene, 80 °C; (b) 1H-Pyrazol-4-ylmethylamine dihydrochloride, DIPEA, methanol, 23% over two steps; (c) Triphosgene, DIPEA, dichloromethane, then oxazol-5-ylmethylamine, 28%.

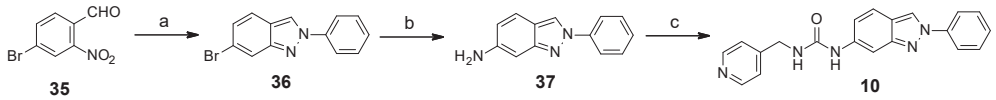

Scheme 4. Synthesis of compound **10**. Reagents and conditions: (a) Tri-*n*-butylphosphine, aniline, 2-propanol, 80 °C, 76%; (b) Benzophenone imine, palladium acetate, 4,5- bis(diphenylphosphino)-9,9-dimethylxanthene, cesium carbonate, 1,4-dioxane, 100 °C then 2 M HCl, THF, 40%; (c) 4-Nitrophenyl [(pyridin-4-yl) methyl]carbamate, triethylamine, 1,4-dioxane, 80 °C, 64%.

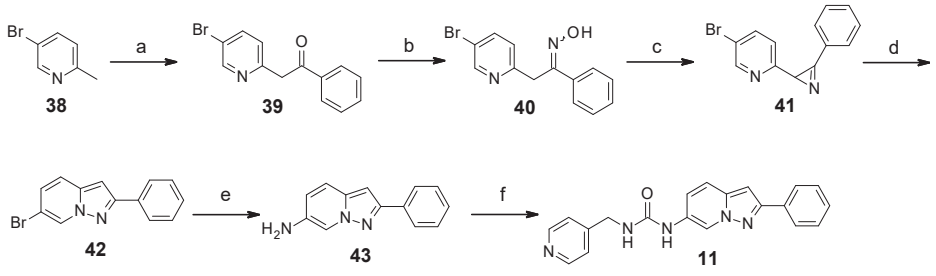

Scheme 5. Synthesis of compound **11**. Reagents and conditions: (a) LiHMDS, THF, −78 °C, then methyl benzoate, 43%; (b) Hydroxylammonium chloride, sodium hydroxide, methanol, 60 °C, 47%; (c) Trifluoroacetic anhydride, triethylamine, dichloromethane, 85%; (d) Iron (II) chloride, dimethoxyethane, 90 °C, 75%; (e) Benzophenone imine, palladium acetate, 4,5- bis (diphenylphosphino)-9,9-dimethylxanthene, cesium carbonate, 1,4-dioxane, 100 °C then 2 M HCl, THF, 58%; (f) 4-Nitrophenyl [(pyridin-4-yl)methyl] carbamate, triethylamine, 1,4-dioxane, 80 °C, 60%.

methyl ester **25** was constructed by amination of the pyridine nitrogen atom of compound **24**,[29] which was followed by condensation with appropriate acyl chlorides, either purchased or generated by reacting the corresponding carboxylic acid with thionyl chloride, or by condensation with the corresponding carboxylic acid utilizing EDCI as a coupling reagent. Compound **25** was then hydrolysed to carboxylic acid **26**. Subsequent Curtius rearrangement of **26,** followed by *in situ* reaction of the corresponding isocyanates with 4-picolylamine afforded urea compounds **12**, **16**–**18**, **22**, and **23**. As an alternative pathway, carboxylic acid **26** was transformed to either aniline **27** or Boc-protected aniline **28** via a Curtius rearrangement, which was further reacted with 4-nitrophenyl [(pyridin-4-yl) methyl]carbamate[30] to give the corresponding urea compounds **15**, **19**, and **20**.

Scheme 2 illustrates the synthesis of pyrazole analog **21**. The triazolopyridine core structure was constructed from pyridine **24** via thiourea **29**, which was subsequently condensed with hydroxylammonium chloride to give **30**.[29] In order to install the right-hand pyrazole ring, the amino group of **30** was converted to the bromine by a Sandmeyer reaction, followed by Suzuki coupling with 1-methyl-1H-pyrazole-5-boronic acid pinacol ester. Subsequent basic hydrolysis and a Curtius rearrangement yielded Boc-protected aniline **32.** Deprotection of the Boc group, followed by urea formation by triphosgene and 4-picolylamine afforded the final compound **21**.

Scheme 3 depicts the synthesis of compounds **13** and **14**. As for compound **13** with a pyrazole group, aniline **27a** was reacted with commercially available 4-nitrophenyl chloroformate to afford the carbamate intermediate **34**, which was coupled with 1H-pyrazol-4-ylmethylamine to afford the final product **13**. Synthesis of compound **14** with an oxazole group was accomplished by treating aniline **27a** with triphosgene followed by coupling with oxazol-5-ylmethyl amine.

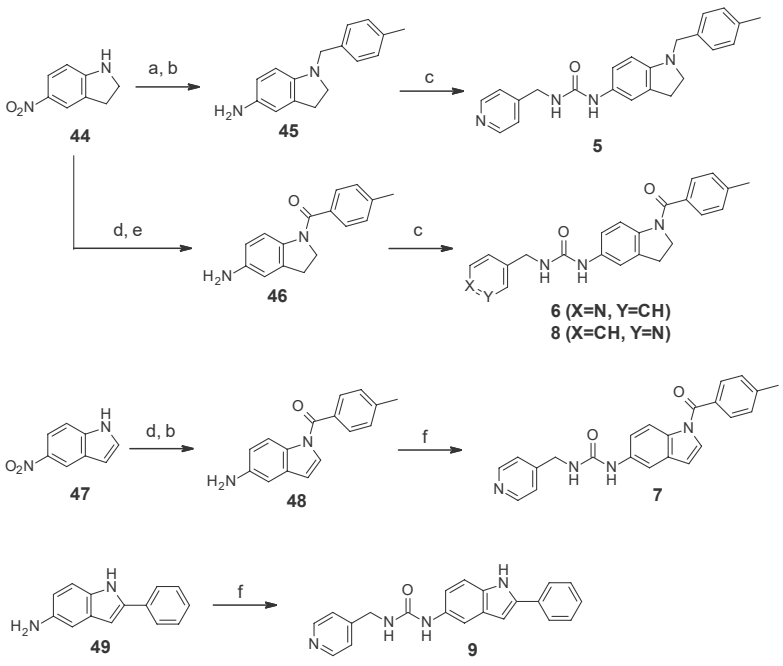

Scheme 6. Synthesis of compounds **5**–**9**. Reagents and conditions: (a) 4-Methylbenzyl bromide, sodium hydride, DMF, ice bath to rt; (b) Iron powder, 2 M HCl, ethanol, THF, 80 °C, 29–44% over two steps; (c) Triphosgene, triethylamine, 4-picolylamine or 3-picolylamine, dichloromethane, 61–73%; (d) *p*-Toluoyl chloride, triethylamine, dichloromethane; (e) H_2, Pd/C, EtOH, THF, 50 °C, 37% over two steps; (f) 4-Nitrophenyl [(pyridin-4-yl)methyl]carbamate, triethylamine, 1,4-dioxane, 60 °C, 45–96%.

Scheme 4 and 5 delineates the synthesis of indazole and pyrazolopyridine derivatives. The indazole core structure of bromide **36** was generated by reductive cyclization of 4-bromo-2-nitrobenzaldehyde **35** as reported by Genung et al (Scheme 4).[31] Pd-catalyzed amination of **36** with benzophenone imine followed by acid cleavage provided aniline **37**, which was converted to the final urea compound **10** by coupling with 4-nitrophenyl [(pyridin-4-yl)methyl]carbamate. As for the pyrazolopyridine derivative **11**, its core structure was constructed following the synthetic route reported by Stevens et al (Scheme 5).[32] Starting material **38** was converted to ketone **39** which was reacted with hydroxylammonium chloride to afford oxime **40**, then subsequently converted to pyrazolopyridine **42** via azirine intermediate **41**. The obtained bromide **42** was transformed to the final urea compound **11** following the procedure analogous to those depicted in Scheme 4.

Synthesis of indoline and indole derivatives **5**–**9** are illustrated in Scheme 6. Starting from commercially available 5-nitroindoline **44** or 5-nitroindole **47**, its nitrogen was either alkylated or acylated, subsequently followed by reduction of nitro group by either iron powder (**45** and **48**) or hydrogenation (**46**). Aniline intermediates were converted to final urea compounds utilizing either the triphosgene method (**5**, **6** and **8**) or carbamate coupling (**7** and **9**). The 2-phenylindole derivative **9** was prepared from the corresponding aniline **49** which was commercially available.

Our initial SAR exploration is summarized in Table 1. For our primary SAR driving assay we utilized human NAMPT enzyme, with activity evaluated by chemically converting the NMN produced by NAMPT to a fluorescent substance, and using the fluorescence intensity as an index of amount of NMN production.[33] The Emax of the synthesized compounds were calculated as percentage of the maximal activity achieved with 30 μM of compound **1**.[34] We also employed a cell-based assay measuring the level of NAD^+ increase in HEK293A cells across a range of concentrations utilizing a NAD/NADH-Glo assay kit. Unfortunately, our initial attempt to simply merge the two structural features of **1** and **2**, the (pyridin-4-ylmethyl) urea moiety and the pyrrolidine ring, resulted in loss of activity (data not shown); therefore, we conducted a further scaffold hopping investigation seeking an alternative structure for pyrrolidine ring. Introduction of a fused bicyclic structure forming an indoline ring resulted in weak NAMPT activation activity (**5**). Furthermore, we were delighted to see that incorporation of amide linker to the side chain of the indoline moiety (**6**) led to stronger activity in NAMPT enzyme assay as well as moderate cellular activity. Converting the indoline ring to indole (**7**) led to stronger potency, though its Emax was lower than that of indoline analog. Moreover, the 3-pyridyl analog of compound **7** elicited a switch in mode of action from NAMPT activation to NAMPT inhibition (**8**).[35] Although compound **7** showed highest activity in NAMPT enzyme assay among these series, the cellular activity was suboptimal, so we decided to further explore the central core region aiming enhancement of activity.

Table 6
Effects on hERG current of compound **12** and **21**.

Cpd	hERG inhibition[a] (%)		
	3 μM	10 μM	30 μM
12	20	51	69
21	11	14	25

[a] % inhibition at given compound concentration.

Our initial attempt focused on the 2-phenyl-1H-indole **9** which showed increased activity in NAMPT enzyme and cell-based assays compared to its *N*-substituted analog **7** (Table 2). Encouraged by this result, we screened nitrogen-containing 6–5 fused bicyclic aromatic rings with a phenyl substituent in a similar position. Among several ring systems we have attempted, indazole (**10**), pyrazolopyridine (**11**) and triazolopyridine (**12**) exhibited potent NAMPT activation activity with increased potency and efficacy. Compounds **10**, **11** and **12** also showed potent activity in the cell-based assay, with the NAD^+ increase exceeding 100% at all the tested concentrations.

The compounds which showed potent activities in NAMPT enzyme and cell-based assays were further profiled to assess their

Table 7
Physicochemical and *in vitro* ADME properties of compound **21**.

ADME properties	Compound **21**
Solubility (pH = 1.2, 6.8) (μg/mL)	>680, 18
Metabolic stability[a] (h, mou) (%)	97, 83
Plasma protein binding[b] (mouse) (%)	30
PAMPA permeability (pH 5.0, pH 7.4) (nm/s)	0.4, 0.8

[a] The % remaining value at 1 μM concentration of compounds reacted with human or mouse microsomes for 30 min.
[b] The % unbound in mouse plasma.

Table 8
Pharmacokinetic parameters of compound **12** and **21** (C57BL/6N mice, po administration[a], 10 mg/kg).

Cpd	Structure	$T_{1/2}$ (h)	Cmax (μM)	$AUC_{0\text{-}24}$ (μM·h)
12	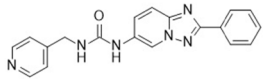	0.9	9.2	25
21	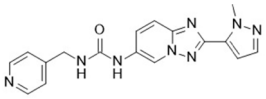	1.9	0.1	0.3

[a] Compounds were administered with 0.5% methylcellulose as a solvent.

physicochemical and *in vitro* ADME properties (Table 3). In general, these compounds exhibited high membrane permeability and metabolic stability in human and mouse microsomes. However, most compounds were associated with CYP direct inhibition (DI) which was presumably caused by the exposed pyridine ring incorporated at the left-hand side, as such heterocycles are typically thought to cause CYP inhibition by binding to the heme center of the CYP enzymes.[36] CYP inhibition was prevalently observed with several NAMPT inhibitors containing an exposed pyridine ring[36] as well as our previously described NAMPT activators. Notably, triazolopyridine analog **12** showed acceptable solubility in the neutral pH, along with attenuated CYP DI for CYP2D6 and CYP3A4. Concomitantly considering the ADME properties and NAMPT activation activity, compound **12** became our lead compound for further SAR around the triazolopyridine template with the aim to see whether attenuating CYP DI while possessing desired levels of NAMPT potency was feasible.

Initially, we explored the left-hand region of our compound, the exposed pyridine ring (Table 4). As this moiety is hypothesized to be crucial for the compound's interaction with NAMPT enzyme, an intensive exploration of this left-hand region previously identified 4-pyrazole and 5-oxazole as heterocycles showing NAMPT activation other than 4-pyridine.[28] 4-Pyrazole and 5-oxazole were also tolerated with this template, displaying optimal activities in NAMPT enzyme and cell-based assays (**13** and **14**). Unfortunately, although decreasing tendency for DI of CYP2C9 and CYP3A4 was observed, CYP1A2 DI could not be attenuated to a desired level.

Having concluded that CYP DI could not be attenuated through conversion of the exposed 4-pyridine ring, we turned our attention to the right-hand region of our compound, where we explored additional structural modifications (Table 5). As for the substituent on the phenyl ring, the ortho position (**15**) was favorable in terms of NAMPT activation activity, whereas meta substitution (**16**) led to decrease of activity, and para substitution (**17**) was detrimental. CYP2C9 DI was consistently observed among these phenyl analogs. As Zak et al. illustrated in their work that increasing the fraction of sp^3 carbon atoms (Fsp^3) was favorable for reducing CYP inhibition,[36] we attempted to introduce aliphatic groups to this region (**18** and **19**), but this resulted in an impairment of NAMPT activation. We subsequently explored installation of heterocycles in the aim of decreasing lipophilicity, for it is commonly known that there is a correlation between CYP inhibition and lipophilicity.[37] Although introduction of an *N*-methylpyrrole (**20**) was tolerated in terms of NAMPT activation activity and reduced the compound's log*D* to 2.6, high CYP2C9 DI remained. Somewhat surprisingly, installing pyrazole ring to this region had a profound effect in reduction of CYP DI; *N*-methylpyrazole analog **21** was an equally potent NAMPT activator, while its lowered log*D* of 1.8 led to a significant reduction of CYP DI to the desired level. A bulkier substituent on the pyrazole ring (**22**) improved cellular activity but was accompanied with higher CYP2C9 DI presumably caused by the increased lipophilicity. Of note, low lipophilicity of compound **23**, which possess a pyrazole ring with a methoxyethyl substituent, also translated to reduced level of CYP DI, which was successfully accompanied by equipotent NAMPT activation activity.

As for compound **21** and lead compound **12**, their human ether-a-go-go related gene (hERG) inhibition was also evaluated (Table 6). Compound **21** exhibited lower tendency of hERG inhibition compared to compound **12**, of which the decrease in lipophilicity may also be a factor.

Physicochemical and *in vitro* ADME properties of compound **21** are shown in Table 7. Compound **21** was highly soluble in acidic medium and exhibited excellent metabolic stability in human and mouse plasma. Compound **21** also exhibited substantial level of free fraction (30%) in mouse plasma. Unfortunately, the low lipophilicity of compound **21** abrogated membrane permeability, which can potentially impact oral bioavailability. Indeed, compound **21** showed lower exposure compared to compound **12** when orally administered to mice (Table 8), indicating additional optimization will be required in order to acquire an optimal compound with a well-balanced overall preclinical profile.

In summary, optimization of HTS hits led to the discovery of (pyridin-4-ylmethyl) urea derivatives with bicyclic core structures that are potent NAMPT activators in both biochemical and cell-based assays. In particular, triazolopyridine **12** was identified as a lead compound, displaying potent NAMPT activation activity and favorable ADME properties albeit with high levels of CYP direct inhibition. Through additional SAR investigation, lowering log*D* was shown to be beneficial for the reduction of CYP inhibition, which yielded compound **21** that had attenuated CYP inhibition along with hERG inhibition. Unfortunately, the low lipophilicity of compound **21** led to low membrane permeability, which translated into poor oral exposure. Further optimization to give compounds with high oral exposure while maintaining low risk of CYP inhibition will be necessary.

Declaration of Competing Interest

The authors declare that they have no known competing financial interests or personal relationships that could have appeared to influence the work reported in this paper.

Appendix A. Supplementary data

Supplementary data to this article can be found online at https://doi.org/10.1016/j.bmcl.2021.128048.

References

1 Xiao W, Wang R-S, Handy DE, Loscalzo J. *Antioxd Redox Signal*. 2018;28:251–272.
2 Imai S, Gurante L. *Trends Cell Biol*. 2014;24:464–471.
3 Canto C, Menzies K, Auwerx J. *Cell Metab*. 2015;22:31–53.
4 Rajman L, Chewalek K, Sinclari DA. *Cell Metab*. 2018;27:529–547.
5 Yang Y, Sauve AA. *Biochim Biophys Acta*. 1864;2016:1787–1800.
6 Verdin E. *Science*. 2015;350:1208–1213.
7 Katsuyaba E, Auwerx J. *EMBO J*. 2017;36:2670–2683.
8 Yoshino J, Mills KF, Yoon MJ, Imai S. *Cell Metab*. 2011;14:528–536.
9 Hershberger KA, Martin AS, Hirschey MD. *Nat Rev Nephrol*. 2017;13:213–225.
10 Lee CF, Chaves JD, Garcia-Menendez L, et al. *Circulation*. 2016;134:883–894.
11 Tran MT, Zsengeller ZK, Berg AH, et al. *Nature*. 2016;531:528–532.
12 Khan NA, Auranen M, Paetau I, et al. *EMBO Mol Med*. 2014;6:721–731.
13 Araki T, Sasaki Y, Milbrandt J. *Science*. 2004;305:1010–1013.

14 Gong B, Pan Y, Vempati P, et al. *Neurobiol Aging*. 2013;34:1581–1588.
15 Jia H, Li X, Gao H, et al. *J Neurosci Res*. 2008;86:2083–2090.
16 Ayoub IA, Lee EJ, Ogilvy CS, Beal MF, Maynard KI. *Neurosci Lett*. 1999;259:21–114.
17 Wang SN, Miao CY. *Stroke Vasc Neurol*. 2019;4:83–139.
18 Lin JB, Kubota S, Ban N, et al. *Cell Rep*. 2016;17:69–85.
19 Williams PA, Harder JM, Cardozo BH, Foxworth NE, John SWM. *Commun Integr Biol*. 2018;11, e1356956. https://doi.org/10.1080/19420889.2017.1356956.
20 Gomes AP, Price NL, Ling AJY, et al. *Cell*. 2013;155:1624–1638.
21 Zhang H, Ryu D, Gariani K, et al. *Science*. 2016;352:1436–1443.
22 Costford SR, Brouwers B, Hopf ME, et al. *Mol Metab*. 2018;7:1–11.
23 Wang T, Zhang X, Bheda P, Revollo JR, Imai S, Wolberger C. *Nat Struct Mol Biol*. 2006;13:661–662.
24 Gardell SJ, Hopf M, Khan A, et al. *Nat Commun*. 2019;10:3241.
25 The maximal NAMPT activation for individual compounds (Emax) in the enzyme assay was determined as a percentage of the maximal activation by 2.5 mM ATP, since ATP phosphorylation of NAMPT H247 causes activation of NAMPT enzyme (see Ref. 26 and 27).
26 Burgos ES, Schramm VL. *Biochemistry*. 2008;47:11086–11096.
27 Burgos ES, Ho M, Almo SC, Schramm VL. *Proc Natl Acad Sci USA*. 2009;106:13748–13753.
28 Pinkerton AB, Sessions EH, Hershberger P, et al. *Bioorg Med Chem Lett*. 2021. https://doi.org/10.1016/j.bmcl.2021.128007.
29 Hamadouchi C, Maiti P, Warshawsky AM, et al. *J Med Chem*. 2018;61:934–945.
30 Christensen MK, Björkling F. WO2010/023307.
31 Genung NE, Wei L, Aspnes GE. *Org Lett*. 2014;16:3114–3117.
32 Stevens KL, Jung DK, Alberti MJ, et al. *Org Lett*. 2005;7:4753–4756.
33 Formentini L, Moroni F, Chiarugi A. *Biochem Pharmacol*. 2009;77:1612–1620.
34 NAMPT activation elicited by **1** reached an Emax plateau at a compound concentration of 30 μM and showed highly reproducible NAMPT activation; thus, we considered it suitable as a standard for calculation of Emax of the synthesized test compounds.
35 This switch in mode of action was also observed with our previous reported NAMPT activators, see Ref. 24 and 28.
36 Zak M, Yuen P, Liu X, et al. *J Med Chem*. 2016;59:8345–8368.
37 Yang Y, Engkivst O, Llinas A, Chen H. *J Med Chem*. 2012;55:3667–3677.